Supplemental Information

Solid-state Sodium Batteries with P2-type Mn-based Layered Oxides by Utilizing Anionic Redox

Steven Kmiec, Panawan Vanaphuti, Arumugam Manthiram*, z

Materials Science and Engineering Program & Texas Materials Institute

The University of Texas at Austin, Austin, Texas 78712, USA

z Corresponding Author E-mail Address: rmanth@austin.utexas.edu

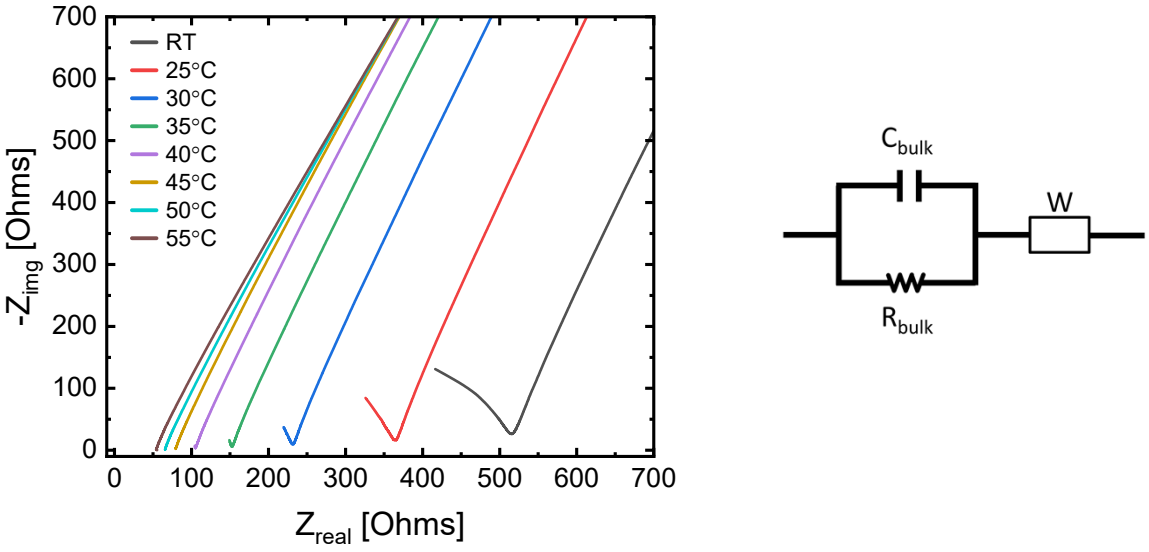

Fig. S1 Temperature-dependent Nyquist plots of the CSE measured from RT to 55°C, alongside the equivalent-circuit model used to extract the resistance values for ionic conductivity measurements.

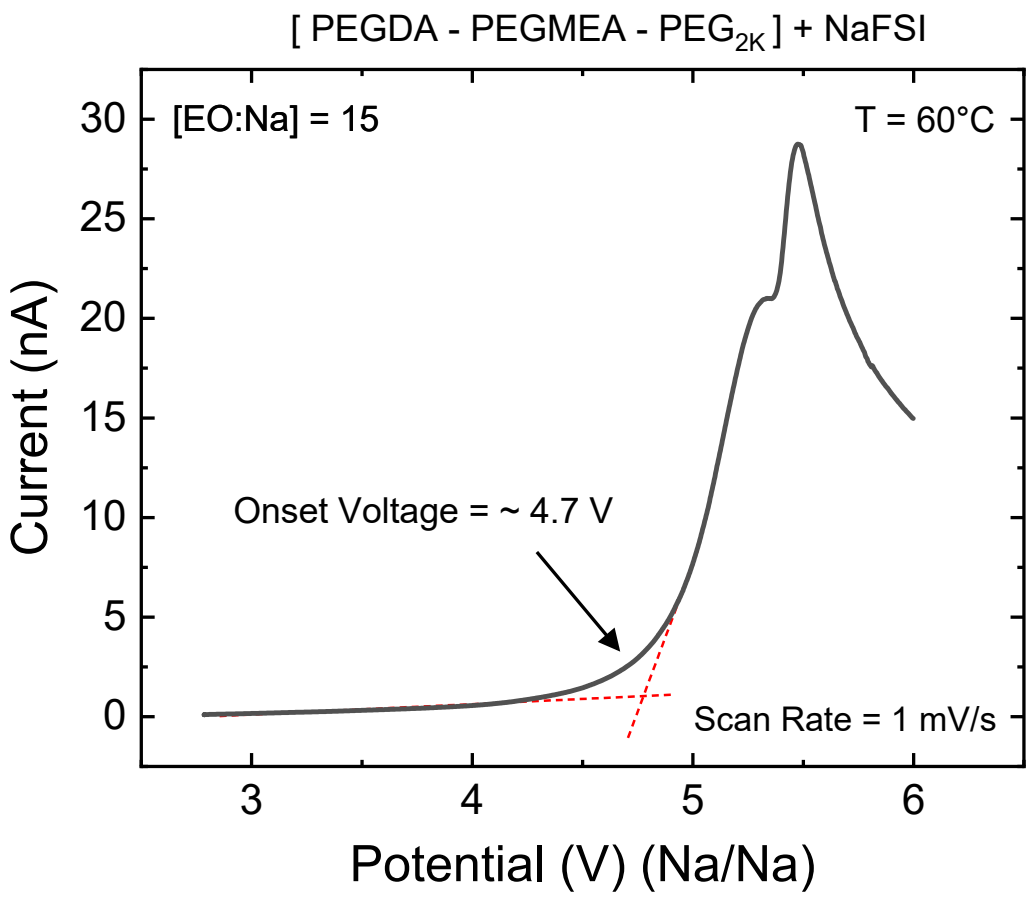

Figure S2. Linear sweep voltammetry measurement of a Na | CSE | SS cell, revealing the upper voltage limit of the electrolyte to be ~ 4.7 V.

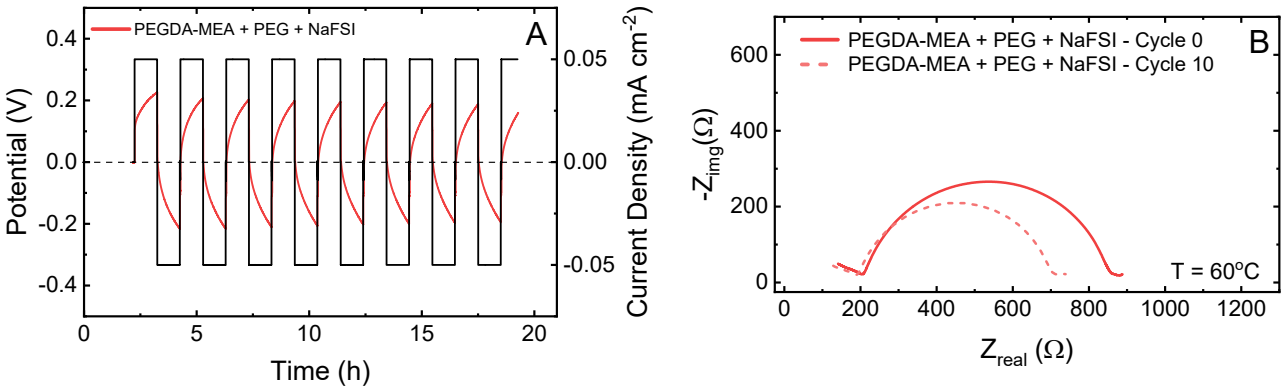

Figure S3. (a) Voltage profiles of Na symmetric solid-state cells cycled with a current density of 50 μA cm^{-2} at 60 °C. (b) Effect of DC stripping/plating on the Nyquist plots of Na | PEGDA-MEA + PEG + NaFSI CSE | Na symmetric cell.

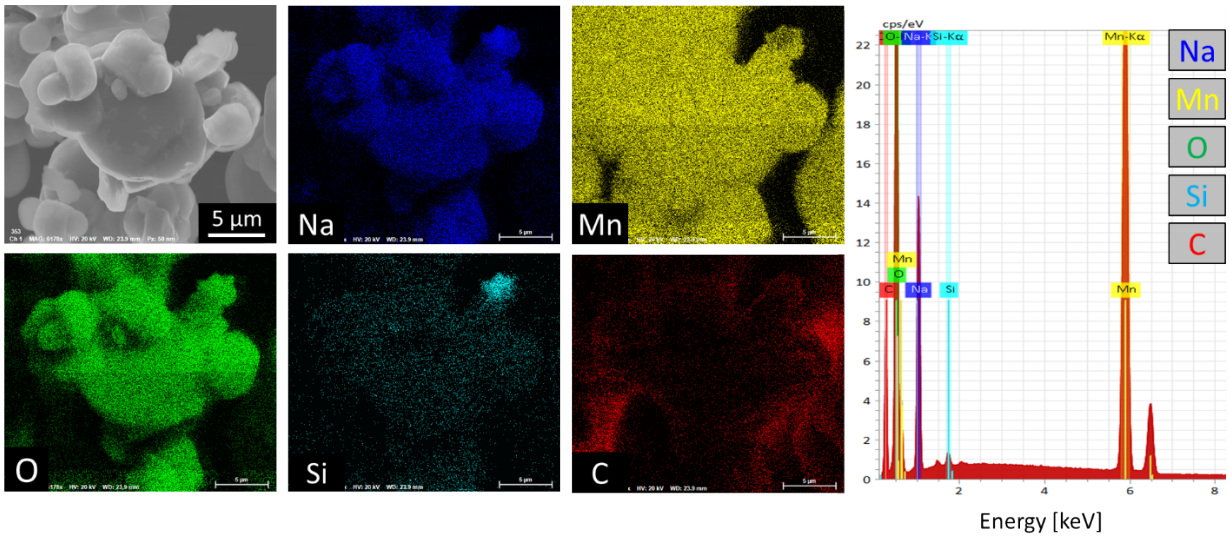

Figure S4. SEM-EDS mapping of pristine Si-NMO powder, confirming the presence of silicon as well as uniform distribution of sodium and manganese throughout the particle. The carbon signal originates from the carbon tape used for sample preparation.

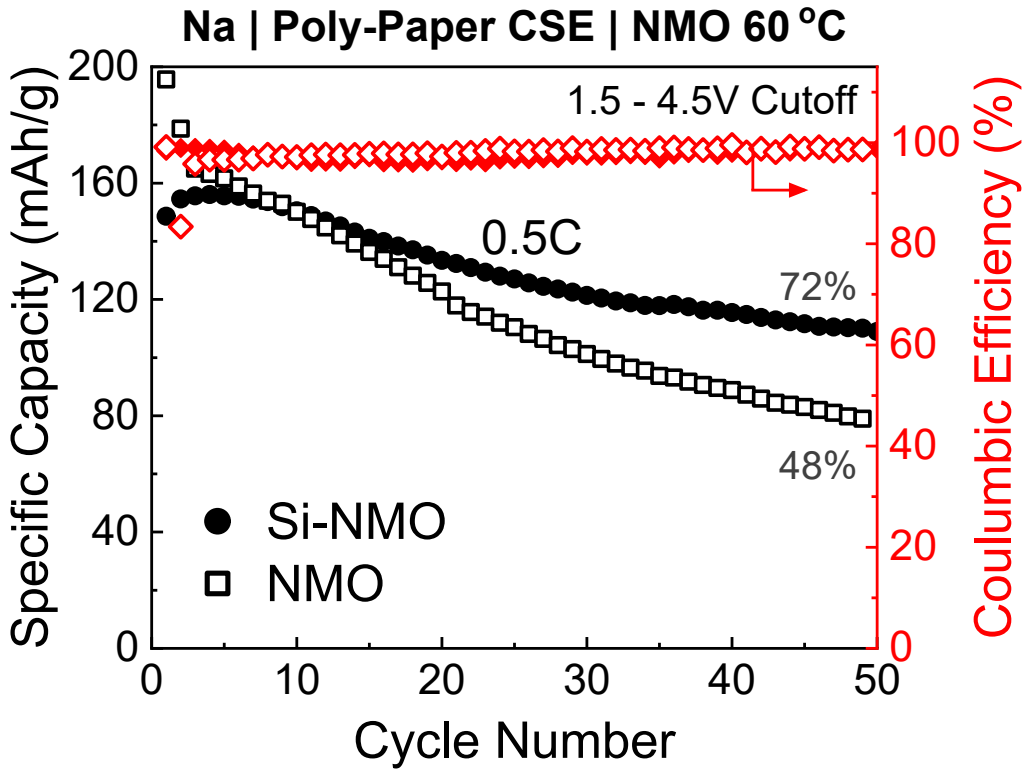

Figure S5. Cycle stability comparison of NMO and Si-NMO based SSSMB with comparable active material loading cycled at a rate of C/2 at 60°C.

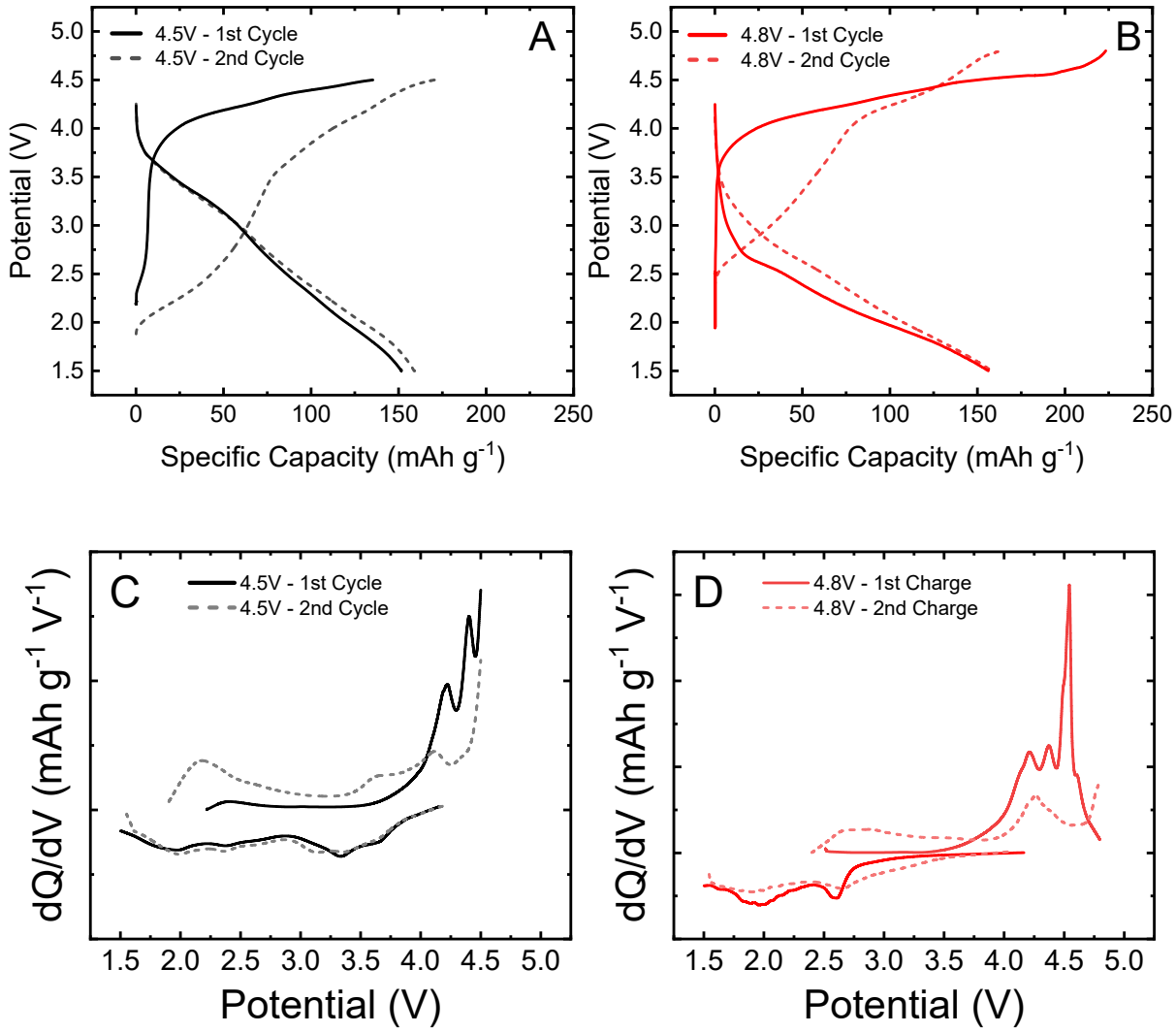

Figure S6. (a-b) First and second cycle voltage profiles of Si-NMO cells with 4.5 and 4.8 V cut-off voltages, revealing for both cells ~150 mAh g^{-1} discharge capacity. Subsequent charge cycles for both cells also produce similar second charge capacities, suggesting the maximum Mn-redox capacity to be ~ 155 mAh g^{-1}. (c-d) Comparison of the 4.5 vs. 4.8 V cut-off voltages on the differential capacity-voltage (dQ dV^{-1}) curves during the first two cycles. All measurements were conducted at 60 ^{o}C in a 2032 coin-cell format.

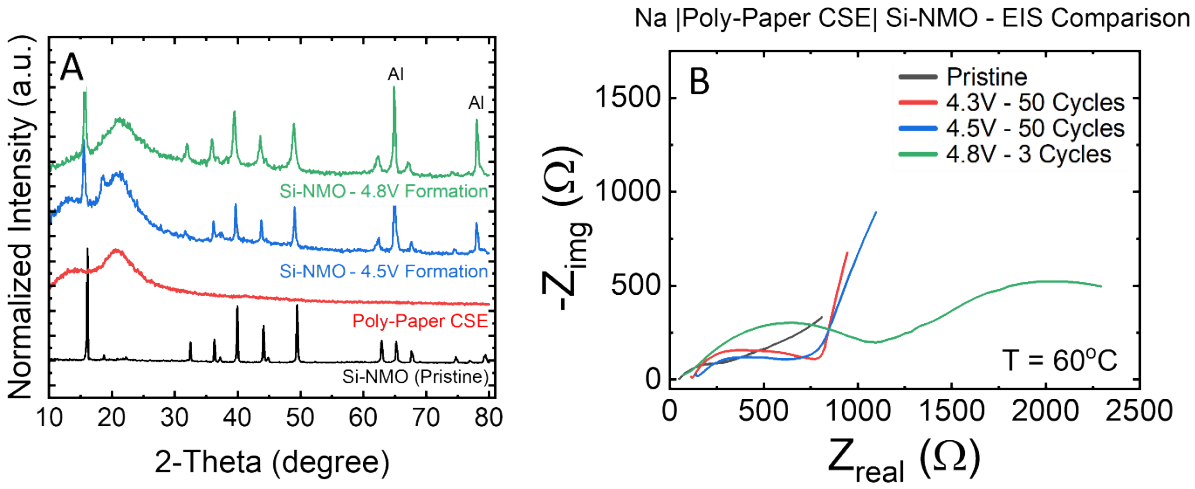

Figure S7. (a) XRD patterns of Si-NMO electrodes after 4.5 and 4.8 V formation cycles. (b) Effect of cut-off voltage on the Nyquist plots of Na | PEGDA-MEA + PEG + NaFSI CSE | Si-NMO cycled cells.

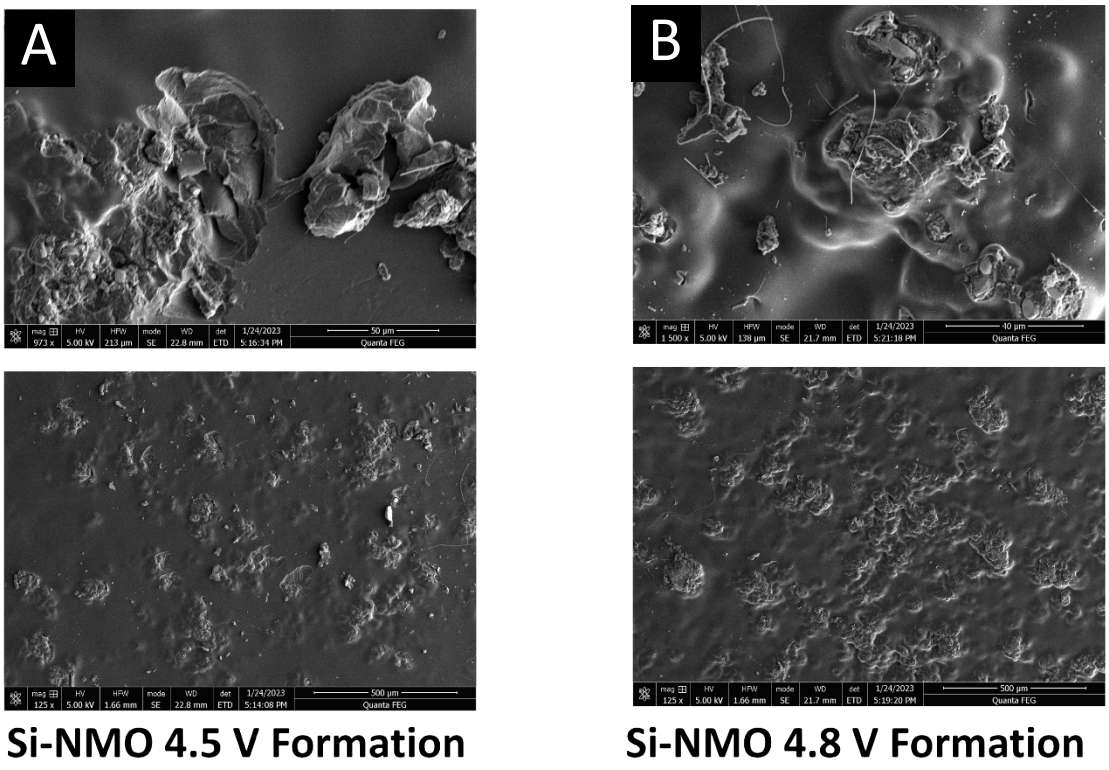

Figure S8. SEM micrographs of the infiltrated electrode surfaces after formation cycles for (a) 4.5 V cut-off, and (b) 4.8 V cut-off. All formation cycles were completed at a charge/discharge rate of C/20 at 60 ºC in a 2032 coin-cell format.

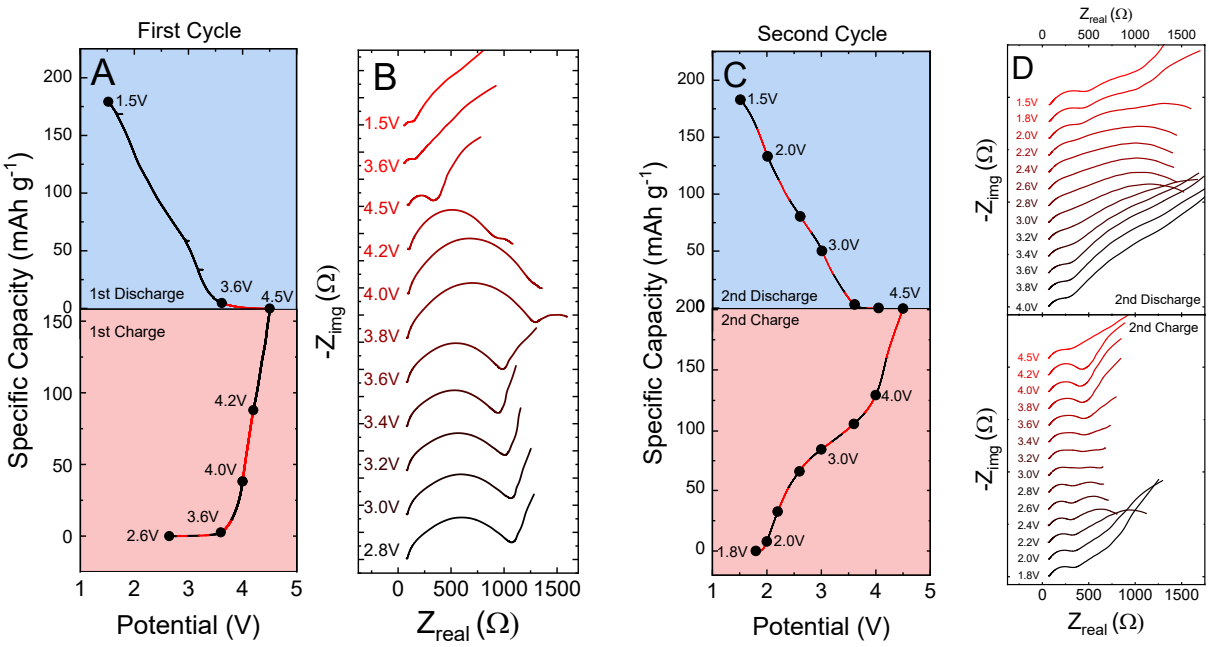

Figure S9. Operando EIS of Si-NMO cells cycled at C/40 rate in a 2032 coin-cells at 60 °C. EIS data were collected every 200 mV, with an excitation voltage of 20 mV. **(a-b)** First charge-discharge cycle and **(c-d)** second charge-discharge cycle curves with corresponding Nyquist plots. All measurements were conducted at 60 °C.

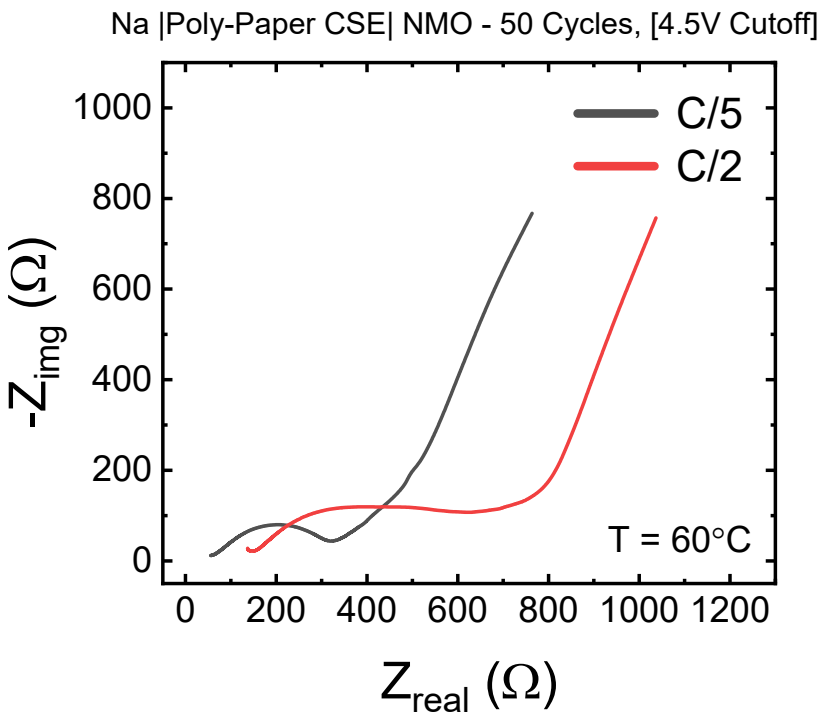

Figure S10. Nyquist plots of Si-NMO cells cycled at different C rates, highlighting the effects of current density on cell resistance. For both cells, the active material loading was held constant at ~ 5.2 mg cm^{-2}.